REPORT SD-TR-88-20

AD-A193 249

Solar Cell Modeling and Simulation

D. C. MARVIN
Chemistry and Physics Laboratory
Laboratory Operations
The Aerospace Corporation
El Segundo, CA 90245

5 February 1988

Prepared for

SPACE DIVISION
AIR FORCE SYSTEMS COMMAND
Los Angeles Air Force Base
P.O. Box 92960, Worldway Postal Center
Los Angeles, CA 90009-2960

DTIC
ELECTE
MAR 0 1 1988
S
D
H

88 2 29 117

This report was submitted by The Aerospace Corporation, El Segundo, CA 90245, under Contract No. F04701-85-C-0086 with the Space Division, P.O. Box 92960, Worldway Postal Center, Los Angeles, CA 90009-2960. It was reviewed and approved for The Aerospace Corporation by S. Feuerstein, Director, Chemistry and Physics Laboratory.

Lt Thomas Wetterstroem/CWASB was the project officer for the Mission-Oriented Investigation and Experimentation (MOIE) Program.

This report has been reviewed by the Public Affairs Office (PAS) and is releasable to the National Technical Information Service (NTIS). At NTIS, it will be available to the general public, including foreign nationals.

This technical report has been reviewed and is approved for publication. Publication of this report does not constitute Air Force approval of the report's findings or conclusions. It is published only for the exchange and stimulation of ideas.

THOMAS WETTERSTROEM, Lt, USAF
MOIE Project Officer
SD/CWASB

RAYMOND M. LEONG, Maj, USAF
Deputy Director, AFSTC West Coast Office
AFSTC/WCO OL-AB

BLANK PAGES
IN THIS
DOCUMENT
WERE NOT
FILMED

REPORT DOCUMENTATION PAGE

1a. REPORT SECURITY CLASSIFICATION	1b. RESTRICTIVE MARKINGS
Unclassified	

2a. SECURITY CLASSIFICATION AUTHORITY	3. DISTRIBUTION / AVAILABILITY OF REPORT
2b. DECLASSIFICATION / DOWNGRADING SCHEDULE	Approved for public release; distribution unlimited.

4. PERFORMING ORGANIZATION REPORT NUMBER(S)	5. MONITORING ORGANIZATION REPORT NUMBER(S)
TR-0086A(2945-01)-6	SD-TR-88-20

6a. NAME OF PERFORMING ORGANIZATION	6b. OFFICE SYMBOL (If applicable)	7a. NAME OF MONITORING ORGANIZATION
The Aerospace Corporation Laboratory Operations		Space Division

6c. ADDRESS (City, State, and ZIP Code)	7b. ADDRESS (City, State, and ZIP Code)
El Segundo, CA 90245	Los Angeles Air Force Base Los Angeles, CA 90009-2960

8a. NAME OF FUNDING / SPONSORING ORGANIZATION	8b. OFFICE SYMBOL (If applicable)	9. PROCUREMENT INSTRUMENT IDENTIFICATION NUMBER
		F04701-85-C-0086-P00016

8c. ADDRESS (City, State, and ZIP Code)	10. SOURCE OF FUNDING NUMBERS			
	PROGRAM ELEMENT NO.	PROJECT NO.	TASK NO.	WORK UNIT ACCESSION NO.

11 TITLE (Include Security Classification)

Solar Cell Modelling and Simulation

12. PERSONAL AUTHOR(S)
Marvin, D. C.

13a. TYPE OF REPORT	13b. TIME COVERED FROM _____ TO _____	14. DATE OF REPORT (Year, Month, Day) 1988 February 5	15. PAGE COUNT 31

16. SUPPLEMENTARY NOTATION

17	COSATI CODES		18. SUBJECT TERMS (Continue on reverse if necessary and identify by block number)
FIELD	GROUP	SUB-GROUP	

19 ABSTRACT (Continue on reverse if necessary and identify by block number)

An important aspect of solar cell design and analysis is the ability to model the wide variety of structures currently under study. This document reports on the application of a modified PISCES semiconductor modeling code that enables nearly all solar cell structures which have been proposed to be simulated, as well as a variety of other opto-electronic devices and processes. Material parameters which may be adjusted include doping profiles, bulk, interface and surface recombination characteristics and contact properties such as ohmic, Schottky, or insulating. Major model selections available include Boltzmann or Fermi-Dirac carrier statistics, voltage or current boundary conditions, and steady-state or time-dependent analyses. Program capabilities are demonstrated by analysis of several state-of-the-art solar cell designs in which the important design parameters are varied and their effect on the cell output parameters shown.

20. DISTRIBUTION / AVAILABILITY OF ABSTRACT	21. ABSTRACT SECURITY CLASSIFICATION
☒ UNCLASSIFIED/UNLIMITED ☐ SAME AS RPT. ☐ DTIC USERS	Unclassified

22a. NAME OF RESPONSIBLE INDIVIDUAL	22b. TELEPHONE (Include Area Code)	22c. OFFICE SYMBOL

DD FORM 1473, 84 MAR   83 APR edition may be used until exhausted. All other editions are obsolete.

CONTENTS

FIGURES

1. INTRODUCTION

An important aspect of solar cell design and analysis is the ability to model the wide variety of structures which are presently under study. This document reports on the application of the Poisson and Continuity Solver (PISCES) semiconductor modeling code to solar cell studies. The original program supplied by Stanford University has been modified to include optical generation processes as required and to correct a number of significant programming errors. In its present form, nearly all solar cell structures which have been proposed can be simulated by PISCES, as well as a variety of other opto-electronic devices and processes. The material parameters which may be adjusted include, but are not restricted to, doping profiles, bulk, interface and surface recombination characteristics, and contact properties such as ohmic, Schottky or insulating. The major model selections available include Boltzmann or Fermi-Dirac carrier statistics, voltage or current boundary conditions, and steady state or time-dependent analyses.
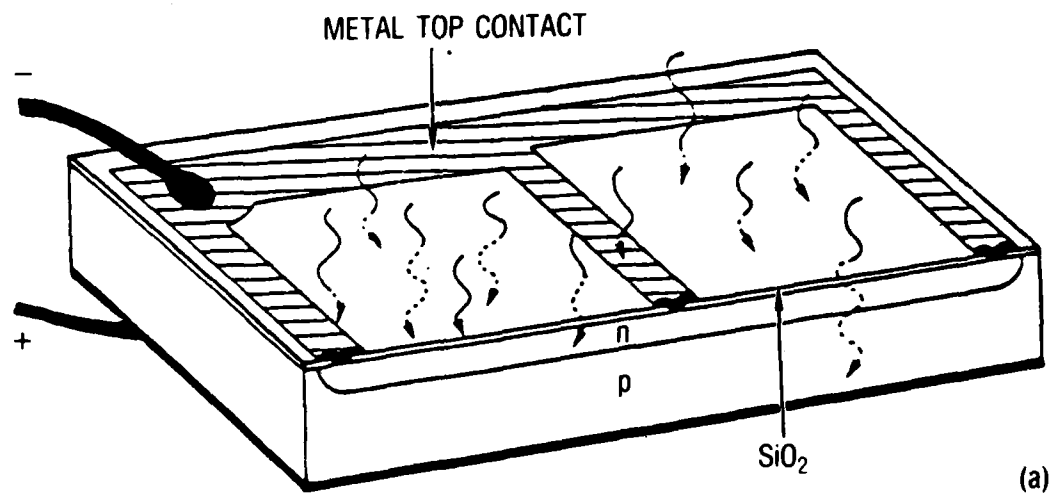
The program capabilities are demonstrated by analysis of several state-of-the art solar cell designs in which the important design parameters are varied and their effect on the cell output parameters shown.
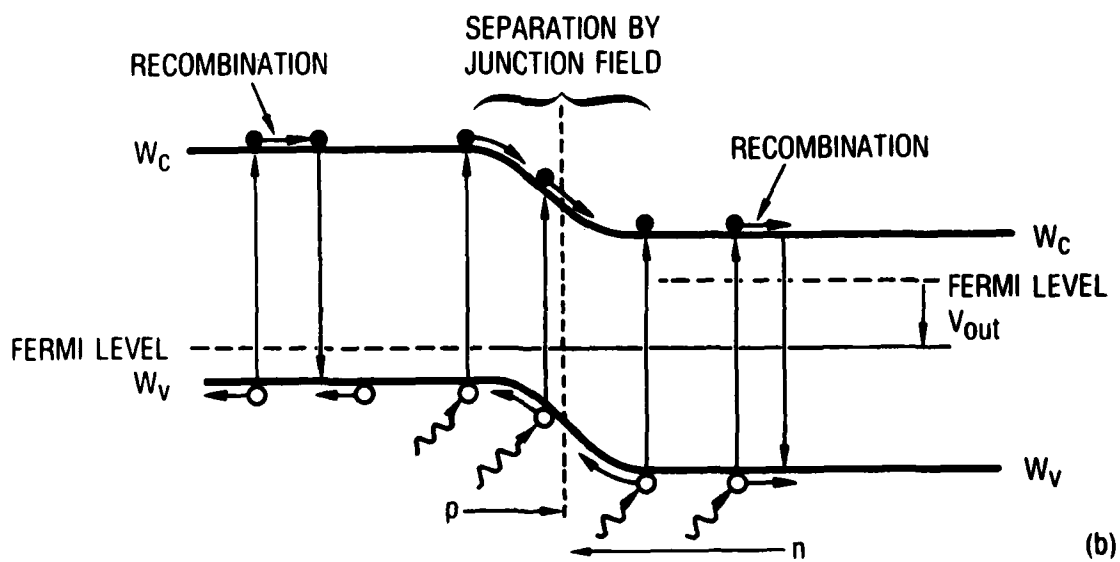
2. SOLAR CELLS

2.1 FUNDAMENTALS

All solar cells consist of a semiconductor material in which an internal electric field causes a depletion region to form. This field can be created by a variety of structures. The major ones include p-n homo- and hetero-junctions, Schottky barriers, metal-insulator-semiconductor structures, and electrolyte-semiconductor interfaces. Figure 1 shows a typical p-n junction device. The internal electric field at the junction serves to spatially separate the photo-generated carriers which are created through the absorption of light. By symmetry, half of the generated carriers are minority carriers which have a limited diffusion length, or lifetime, during which they must move across the junction or be lost via recombination. The efficiency with which the device can cause transport of these carriers to the region where they become majority carriers and then deliver them to their respective terminals, without allowing recombination to occur, is the fundamental measure of device quality. Other basic design options include choice of semiconductor bandgap, which determines the amount of light actually absorbed, and the option of using multiple p-n junctions. However, the most significant advances in solar cell electrical output have occurred through novel methods of maximizing the carrier collection efficiency.

The recombination mechanisms that reduce the cell quantum efficiency can occur in the depletion region, on either side of the junction (emitter or base), in the quasi neutral regions, at the surfaces, and at the ohmic contacts. Reduction of the recombination rates is not simply a matter of successfully executing an ideal design in the laboratory but is rather a series of compromises between competing effects. An example for the case of p-n junction devices is the choice of doping level in the emitter (the upper-most active region of the device where light enters). Heavy doping produces a number of desirable effects including low electrical resistivity which reduces internal voltage drops, band bending effects which produce internal fields that aid in minority carrier collection (referred to as selective ohmic

7

METAL TOP CONTACT

n

p

SiO$_2$

(a)

(a) TOP CONTACT DESIGN

RECOMBINATION

SEPARATION BY
JUNCTION FIELD

RECOMBINATION

W$_c$

W$_c$

FERMI LEVEL

FERMI LEVEL

V$_{out}$

W$_v$

W$_v$

p

n

(b)

(b) ENERGY BAND DIAGRAM

Fig. 1. Typical p-n Junction Solar Cell

8

contacts), and easy ohmic contact formation. The penalty is that the minority carrier lifetime is strongly dependent on doping level, and, therefore, the diffusion length of these carriers is reduced substantially by heavy doping. Thus a compromise is usually made. Complicating this optimization is the option of reduced emitter thickness which, in turn, relaxes the diffusion length requirement.

In the example calculations presented later, the surface recombination is treated as a parameter to demonstrate its effect on cell efficiency. Also the recombination properties of the ohmic contacts are treated. Ideally, such contacts have an infinite recombination velocity for majority carriers and zero recombination for the photogenerated minority carriers. The degree to which this is achieved determines the "selectivity" of the contact. These issues illustrate the rich variety of solar cell design problems which cannot be evaluated properly without the use of a quantitative numerical model.

2.2 DEVICE PARAMETERS

The two major categories of parameters that determine a solar cell's design are device structure and material properties. This discussion will refer specifically to p-n junction devices, but similar considerations apply to all cell types. In the former category, the most basic choices are p/n or n/p emitter/base design, emitter and base thickness and doping, surface passivation method, and contact design.

The region thicknesses are dictated by the absorption coefficient of the material in the spectral region of interest and by the carrier diffusion lengths which can be achieved. Solar cells fabricated from direct bandgap III-V compounds need only be 1-5 μm thick because of their high absorption coefficient. Single crystal Si cells are generally greater than 100 μm thick as a result of the low absorption coefficient of this indirect gap semi-conductor. Amorphous Si alloy cells are comparable in thickness to the direct gap cells because they have a large density of intragap states which are effective absorbers.

9

The previous section described the considerations which affect the selection of doping levels in the emitter region. The base region doping considerations differ in that relatively little light absorption occurs there, especially in III-V bases cells. Therefore, relatively few minority carriers will exist in the base, and the primary loss mechanism will be IR induced voltage drops across the base. An additional loss would arise from increased dark (reverse) current flow.

The selection of ohmic contact structure is also quite important because the contact regions influence the cell operation in several ways. Front contacts usually are a metal grid pattern which represents a compromise between shadowing losses and IR voltage drop caused by excessively narrow metal lines. The back surface has complete ohmic metal coverage, except for cases where infrared transmission by the rear surface is needed to reduce the cell operating temperature. The primary function of the ohmic contact is to collect the majority carriers out of the device into metal grid lines with no significant voltage drop. Generally this is achieved by producing heavily doped n+(n) or p+(p) junctions through which electrons or holes may tunnel, respectively. An added advantage of this type of contact is that a slight grading can provide an electric field near the contact which repels diffusing minority carriers and prevents them from recombining at the contact. Contacts with such fields are described as being "selective". However, selective contacts may also be achieved by using suitably chosen heterojunctions, and thereby avoid an important shortcoming of heavily doped contacts. As mentioned above, the rate of bulk Shockley-Read-Hall (SRH) recombination in the bulk increases rapidly with doping, and, therefore, such contacts always involve a compromise in the choice of dopant concentration. Another method is the introduction of fixed charges of the appropriate sign on the emitter surface between the grid lines so as to repel the minority carriers while attracting majority carriers to the contact.

Two revolutionary contact schemes have been introduced recently that nearly double the output of silicon solar cells. These are the point contact cell (PCC) and the interdigitated backside contact cell (IBC). Both designs reduce SRH and Auger recombination rates by reducing the heavily doped contact

10

area in the cell and by using very low doping for the carrier diffusion region. Substantial increases in open circuit voltages are also obtained through this reduction in contact area. The improvement achievable with these designs was only realized through extensive modeling studies which quantified the tradeoff between reduced loss at the contacts and the more stringent requirements placed on minority carrier diffusion length.

The specification of a solar cell design thus involves a number of basic choices, followed by detailed optimization of the device parameters. Although analytical models are available which treat solar cell operation within certain regions of operation, general analyses require a two- or three-dimensional numerical solution method. The PISCES solution method can treat all of the important two-dimensional effects in solar cells. The relevant parameters and porcesses are specified as input, and values for the experimental observables are produced as part of the output.

2.3 EXPERIMENTAL OBSERVABLES

The processes which limit solar cell efficiency, such as bulk and interfacial recombination, can only be observed directly by rather sophisticated techniques. These methods are indispensable for process evaluation as well as degradation analysis; however, they are not used routinely. The most commonly used diagnostic method is the current-voltage measurement. Figure 2 shows a typical current-voltage curve and identifies the short circuit current density J_{sc}, open circuit voltage V_{oc} and maximum power point (V_m, J_m). From these the fill factor $FF = V_m J_m / V_{oc} J_{sc}$ and overall efficiency $\eta = V_m J_m / P_{in}$ may be computed, where P_{in} is the total incident optical power. The symbol J denotes current density in amps/cm^2 while I is current in amps. An absolute upper limit on solar cell output is set by the bandgap E_g, since this determines the fraction of P_{in} which can be absorbed. These limits are approximately 41% for GaAs and 43% for Si, respectively.[1] Some cell defects cause well-known variations in the I-V behavior and are thus pinpointed by this diagnostic method. Dark I-V and spectral response measurements assist in deciphering more complex effects.
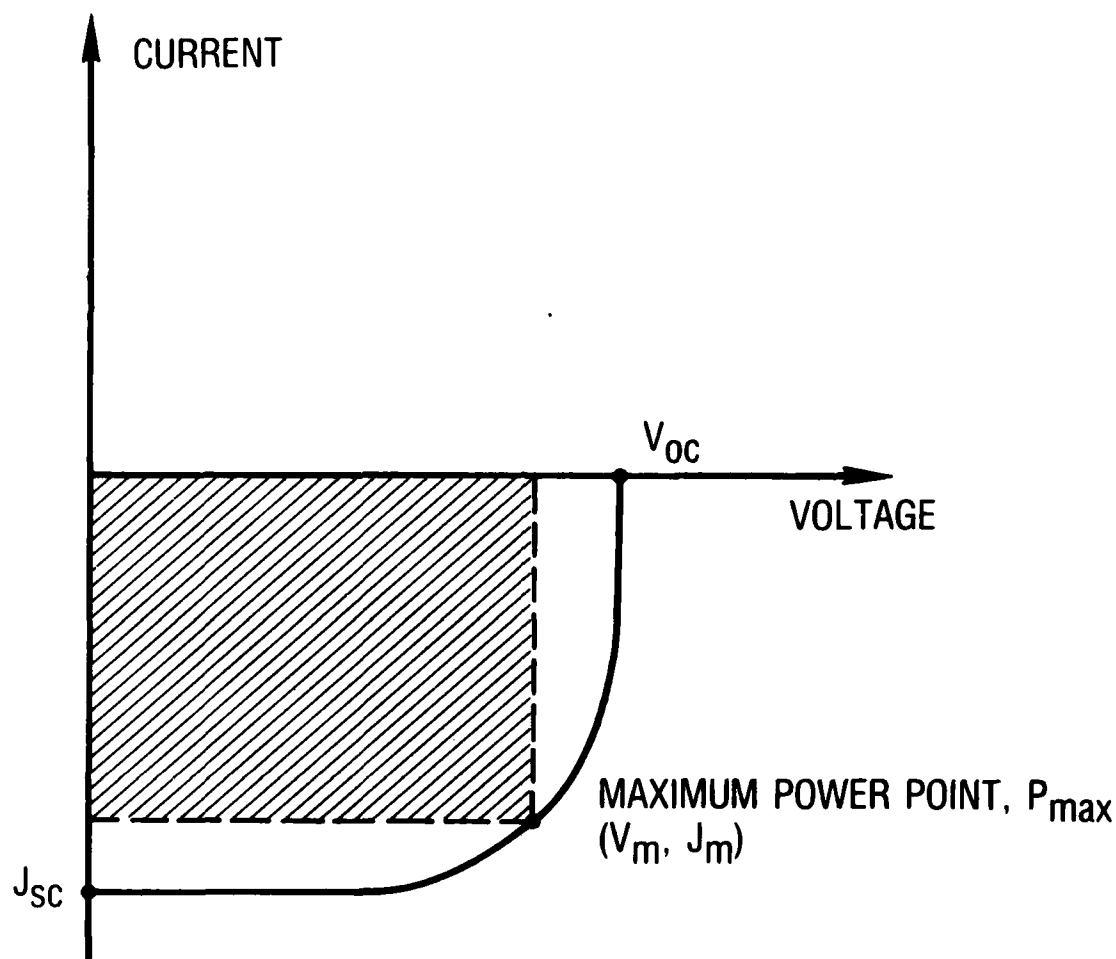
Fig. 2. Typical I-V Curve

Certainly from a design standpoint, the I-V curve is the most widely used predictor of cell behavior. The PISCES code is capable of predicting illuminated I-V behavior, dark I-V bethavior, and spectral response, which will be used in the following sections to demonstrate the effects of parameter variations on cell performance. PISCES is also able to generate transient response data for arbitrary cell designs which may then be used to interpret direct measurements of carrier dynamics.

3. PISCES

The PISCES program is basically a two-dimensional, finite-element, differential equation solver. The fundamental semiconductor differential equations relevant to device analysis

$$\varepsilon \nabla^2 \psi = - q(p - n + N_D - N_A) - \rho \tag{1}$$

$$q \partial n / \partial t = \nabla J_n - U_n + G_n \tag{2}$$

$$q \partial p / \partial t = \nabla J_p - U_p + G_p \tag{3}$$

where

ψ = potential

ε = dielectric constant

q = electron charge

p = hole concentration

n = electron concentration

N_D = ionized donor concentration

N_A = ionized acceptor concentration

ρ = fixed charge density

J = current

U = carrier recombination rate

G = carrier generation rate

are Poisson's equation and the continuity equations, respectively. The solution of these equations comprises self-consistent values for the potential and carrier concentrations. The utility of PISCES arises from the

broad array of processes and parameters, which may be used to supplement these deceptively simple expressions, and the powerful solution algorithms which give remarkable convergence rates. Examples of processes which may be included in the device model are Shockley-Read-Hall, Auger, interface and selective contact recombination, concentration dependent mobilities, bandgap narrowing, Fermi-Dirac carrier statistics, and incomplete impurity ionization. Material parameters such as dielectric constant, band edge state densities, carrier mobilities and lifetimes, interface fixed charges, and impurity energies are adjustable.

Several solution schemes may also be specified. The simplest is a steady-state set of voltage boundary conditions, one for each electrode on the device. The output will then consist of terminal currents, and potential and carrier concentration data at the interior node points. A straightforward extension of this provides output for an applied voltage ramp. Thus, device characteristic curves, such as light and dark I-V curves, can be generated automatically with separate output files for each voltage boundary condition. Alternately, current boundary conditions may be specified in which case terminal voltages become part of the solution. This can be tricky in cases where surface recombination is specified since the recombination rate enters in the form of a current boundary condition.

Transient analysis is also available through specification of time dependent boundary conditions. The time step selection is done automatically, and an output data set is generated for each step. The original PISCES IIb program did not include the generation term G in the continuity equation. The code has been modified to allow optical generation of carriers at arbitrary rates as a function of position. This method was originally used to model latchup phenomena in integrated circuits induced by high energy particles.[2] In the case of opto-electronic devices, it can be used to generate spectral response curves as well as to observe intensity dependent effects. This capability has been used to analyze transient reflectivity experiments applied to carrier relaxation effects in GaAs.[3]

Generally, a specified problem is solved in two Cartesian dimensions which are usually taken to be one lateral dimension and depth. The other lateral dimension is assumed to have a fixed value. For many problems involving laser excitation of samples or radiation effects, there is cylindrical symmetry. In order to take advantage of this, PISCES has been modified to work optimally with cylindrical coordinates rather than Cartesian coordinates. For such problems, the solution is now quite accurate because it has the same dimensionality as the problem.

4. SIMULATION RESULTS

4.1 BASELINE SOLAR CELL STRUCTURE

As a demonstration of the importance of solar cell modeling in design and analysis, a number of simulations are presented below. The parameters chosen for study are especially relevant to current state-of-the-art designs, and comprise surface and bulk recombination, emitter doping and light intensity (for concentrator cells). In each case the effect of parameter variation on V_{oc}, J_{sc}, FF, and η are given.

The baseline cell structure is shown in Figure 3. The cell is a p on n type with a 0.5 μm thick emitter on a 9.5 μm thick base. The metal grid structure covers approximately 10% of the total cell surface area which is somewhat greater than for state-of-the-art cells. This was done in order to avoid the need to provide PISCES with a very fine node spacing under the

METAL
OHMIC CONTACT

PASSIVATION

EMITTER
p-GaAs 10^{18}

0.5 μm

BASE
n-GaAs 5×10^{17}
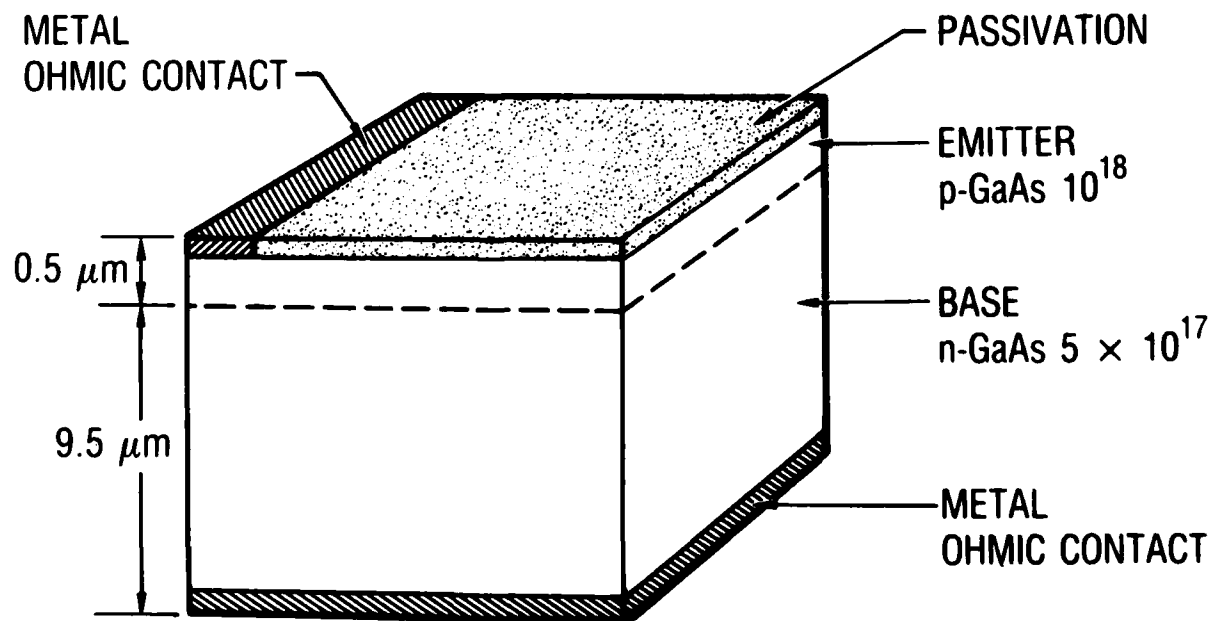
9.5 μm

METAL
OHMIC CONTACT

Fig. 3. Baseline Cell Structure

contact. The light spectrum used for illumination is based on the Air Mass 0 solar spectrum. This spectrum is combined with the known GaAs absorption spectrum to produce a function G(z) which is the carrier generation rate at the depth z. A four parameter fit provides a satisfactory approximation to AMO in GaAs:

$$G(z) = \exp[a0 + a1*z + a2*\exp(a3*z)]$$

where a1,a3 < 0. The optical generation rate in the cell under this approximation is 25.1 mA/cm^2, whereas the true AMO spectrum supplies 39 mA/cm^2. Thus the current densities achieved in these simulations will be somewhat lower than those appropriate for true AMO illumination. In order to avoid confusion, all cell output powers will therefore be given in arbitrary units.

PISCES must be provided with a node system which defines the solution points for the finite element method. The generation of this mesh is the most critical part of the simulation since an inadequate mesh design can lead to convergence problems, inaccuracies and excessive run times. Clearly a low density of nodes is appropriate in regions of the devices where conditions are relatively uniform. Higher densities are required where large carrier gradients or electric fields are present. In order to assist in identifying these regions, PISCES has an automatic node generation option which regrids based on variations of selected parameters. GaAs solar cells place rather stringent requirements on the node mesh since heavy carrier generation occurs in the top micron or so, a large electric field exists at the p-n junction, and large currents flow at the edge of the upper ohmic contact. A portion of the node layout used in these simulations is shown in Fig. 4.

4.2 SURFACE RECOMBINATION AND SOLAR CONCENTRATION

The previous discussion indicated that efficient collection of optically generated carriers is the primary goal of any solar cell design. The most important material parameters in this respect are the bulk minority carrier lifetime τ and the surface recombination velocity S. The lifetime τ effectively defines the characteristic distance L which a minority carrier can
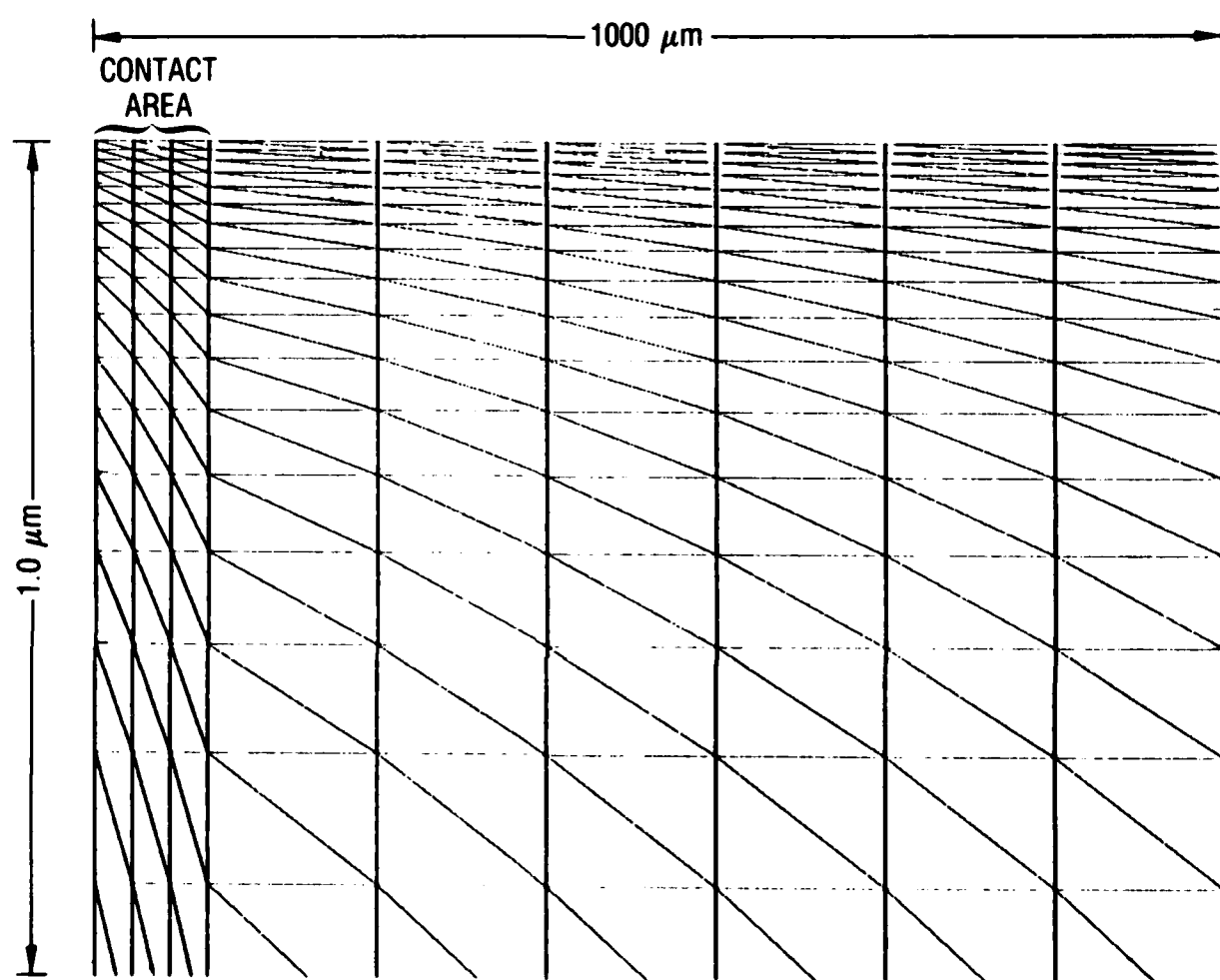
18

Fig. 4. PISCES Node Pattern

diffuse without recombining. If the characteristic lengths of the solar cell are comparable to or exceed L, then less than 100% internal quantum efficiency will be obtained. (In this context, internal quantum efficiency refers to the output current produced per absorbed photon.) Figure 5 shows the output power P_{max} expected from the test structure (Fig. 3) as a function of τ. The upper scales show the diffusion lengths for electrons and holes derived from the assumption that $\tau_p = \tau_n$. The more rapid decrease in P_{max} at short τ occurs because $L_p \leq 10$ μm which is the base thickness across which minority holes must diffuse, and $L_n \leq 0.6$ mm which is the corresponding emitter thickness for minority electrons. Thus both minority holes and monority electrons are being lost to recombination. The weaker dependence of P_{max} on τ at longer times occurs because only the former condition is true. Analysis of this type is central to cell design evaluation because it reveals the optimum region thicknesses and dopings. Refinements of the procedure used here would include the use of distinct lifetimes for each carrier type and concentration dependent lifetimes.

The surface recombination velocity S is the proportionality constant between excess carrier density and concentration gradient at an interface,

$$J_{s,n} = qS_n^*(n_s - n_{eq})$$

$$J_{s,p} = qSp^*(p_s - p_{eq})$$

A large value of S indicates that the surface is an important sink for carriers. Figure 6 shows the effect of S on V_{oc} and P_{max} for the model cell structure at different concentration ratios. The one sun (labeled 1X) results show a strong loss in V_{oc} and P_{max} for $S > 10^4$ cm/s. An unpassivated GaAs surface has S approximately equal to 10^6 cm/s, while one covered with AlGaAs might have S approximately equal to 10^4 cm/s. At 100 suns the effect of increased S on P_{max} is less even though V_{oc} behaves similarly to the 1 sun case. This is caused by the absolute value of V_{oc} starting out higher at S = 0. Generally a larger V_{oc} is achieved in a given cell design where the carrier concentration is increased. The model cell is not a good concentrator design
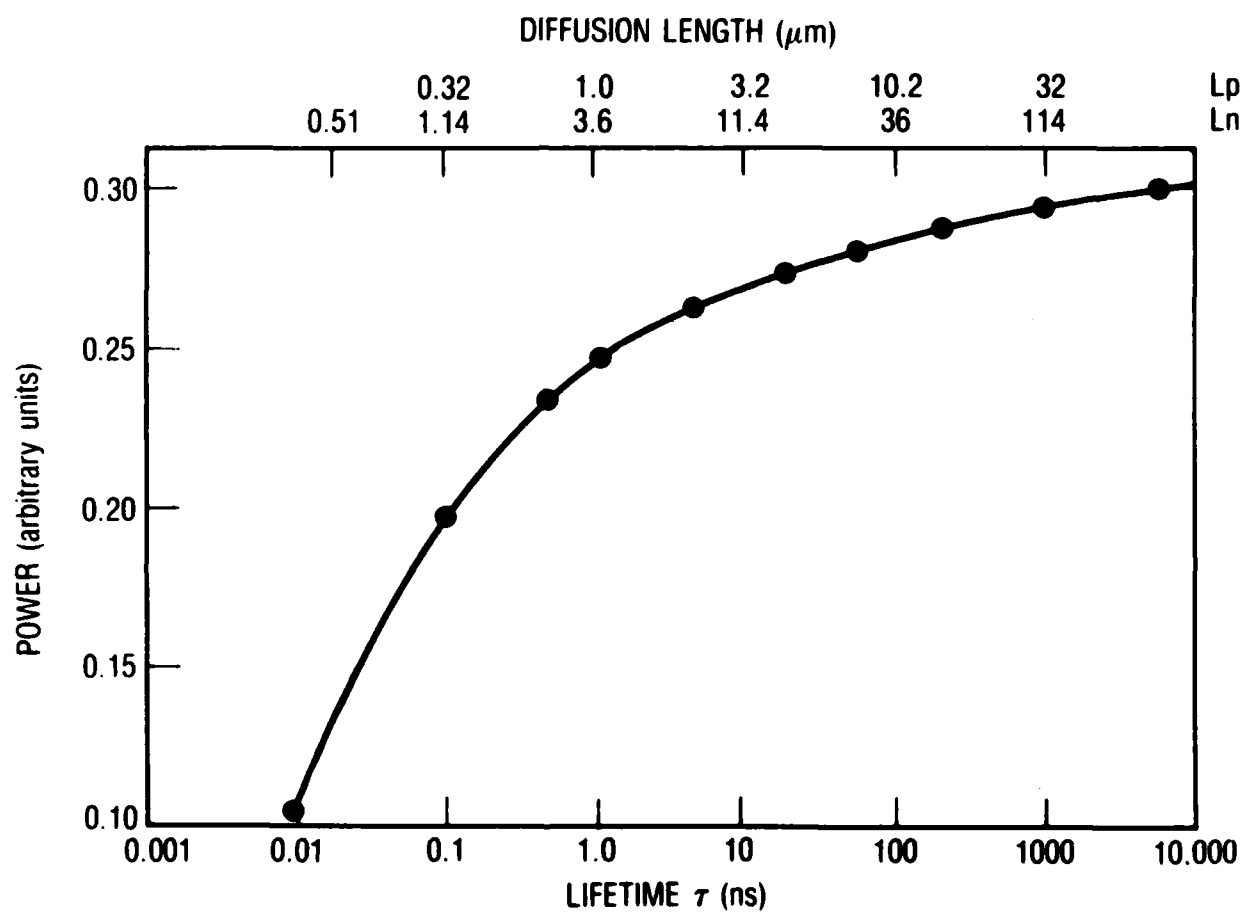
20

DIFFUSION LENGTH (μm)

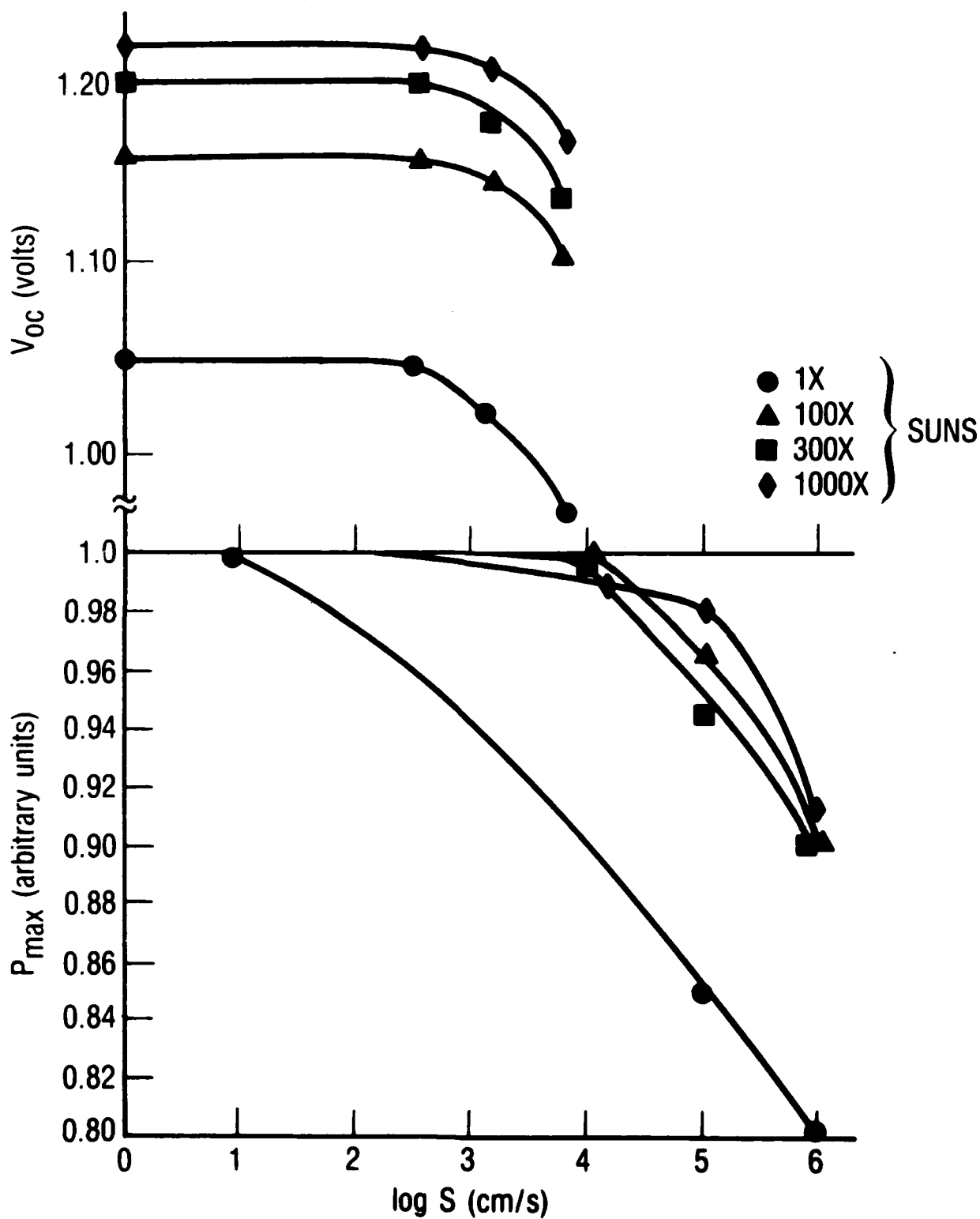Fig. 5.   Power vs. Bulk Lifetime

Fig. 6. Power and Voltage vs. Surface Recombination Velocity

22

because significant power is dissipated in the emitter. A good design would have a more heavily doped emitter and more closely spaced grid lines, which would result in reduced IR voltage drops.

4.3 SPECTRAL RESPONSE

A very useful diagnostic for determining the limiting features of a design is the spectral response characteristic. The blue and red response of a cell can be shown to depend on S and τ, respectively. High energy photons are absorbed near the upper emitter surface where the generated carriers are susceptible to surface recombination. Low energy photons are absorbed more uniformly throughout the base region, and the generated carriers must diffuse some fraction of the base thickness in order to reach the junction and become majority carriers. Figure 7 shows the internal quantum efficiency of the model cell as a function of wavelength for several sets of material para- meters. All of the plots are normalized with respect to the S = 0, τ = ∞ case (i.e., no surface or SRH recombination). The dots indicate the response of a cell with τ = 20 ns. The only effect is at long wavelengths where some car- riers must diffuse across distances comparable to the base width and cannot do so with 100% QE because L is approximately 5 μm while the base thickness is 9.5 μm. The circles indicate results for τ = 20 ns and S = 10^6 cm/s. Here the blue response has degraded substantially due to the essentially unpassi- vated emitter surface. The crosses mark the response of a cell with τ = 20 ns and S = 10^5 cm/s, which is an intermediate case representative of a commercial cell suffering from processing difficulties.

4.4 SELECTIVE OHMIC CONTACT

A "selective" ohmic contact has a high recombination rate for majority carriers and a lower rate for minority carriers. The advantage of this feature is that recombinative losses of minority carriers in the emitter region of the solar cell under the contacts is reduced. Alternatively, an effective field which results from the carrier distribution near an ohmic contact can cause minority carriers to drift toward the junction. Typically this effect is achieved by using either band bending or heterojunctions to selectively repel minority carriers away from the contact, but is then
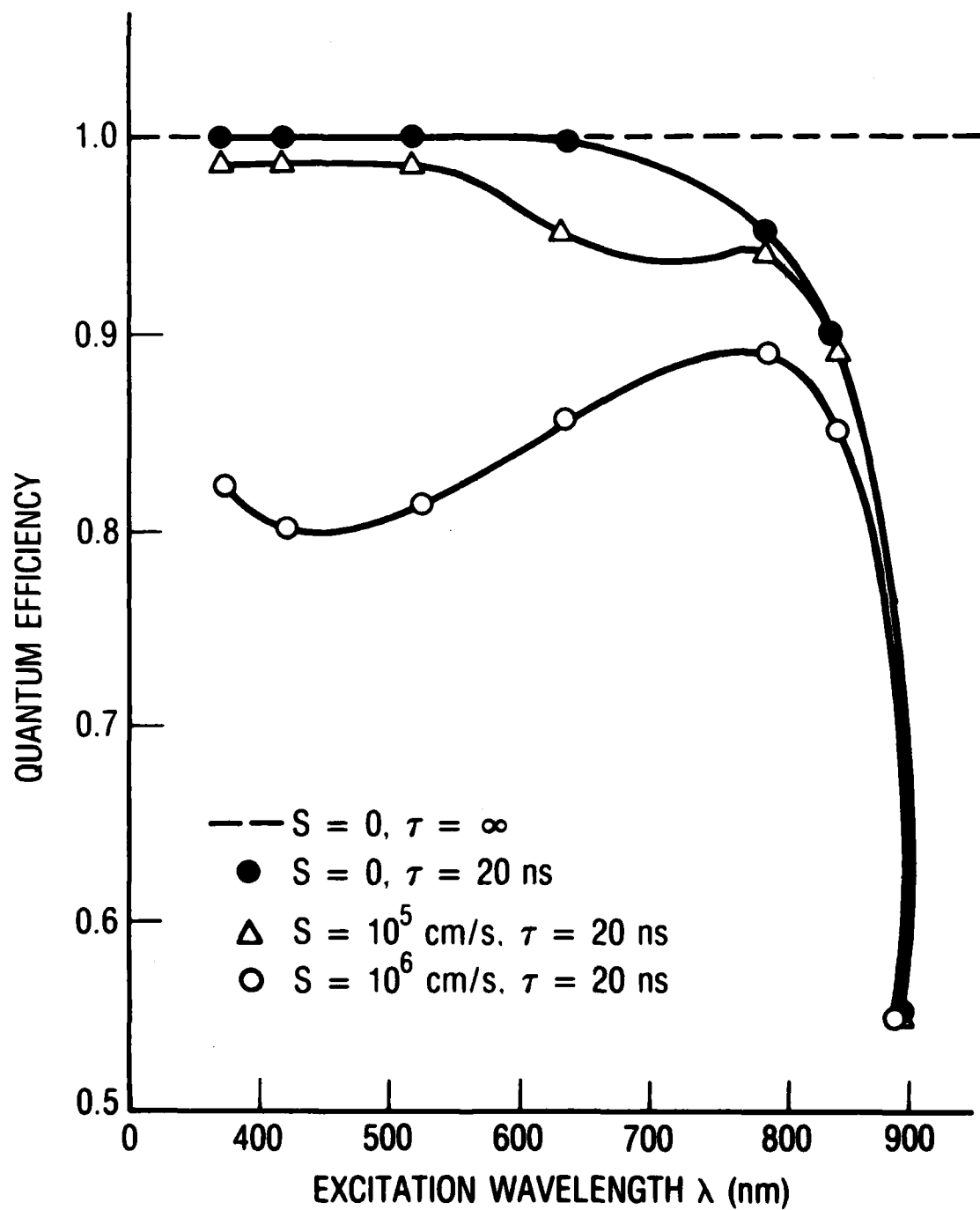
23

Fig. 7. Spectral Response Data

referred to as a "selective" contact as if actual alteration of the contact's properties had occurred. Figure 8 shows the V_{oc} and P_{max} for the baseline cell design with no surface recombination, and majority/minority contact recombination velocities of $10^6/10^2$, $10^6/10^4$, and $10^6/10^6$. A 5% improvement in output power is obtained across this range.

4.5 FRONT SURFACE FIELD

An alternative to front surface passivation as a means of reducing minority carrier losses is the establishment of a drift field in the emitter to repel carriers from the top surface. In the model device used here, electrons are the minority carriers in the emitter so a negative fixed charge on the front surface would be required. Figure 9 shows the effect of fixed charges ranging from $+ 10^{11}$ cm^{-2} to $- 8 \times 10^{11}$ cm^{-2} on V_{oc} and P_{max}. A 7% improvement in power is obtained for the $- 8 \times 10^{11}$ cm^{-2} case. Typical surface state densities on GaAs are 10^{12} cm^{-2} which is more than adequate. The challenge is to create a charged surface with the correct sign. A p-type GaAs surface will have a positive charge due to surface states, which is the wrong sign for the desired effect. Therefore, the surface must be modified to produce negative states (or the positive charges overwhelmed). Recent work on Fermi level unpinning in III-V materials has increased the chances for success in this approach.

4.6 TRANSIENT ANALYSIS

Information may also be obtained on the carrier recombination processes by making time resolved measurements. One such technique which is useful for p-n junction devices is the Time-of-Flight (TOF) measurement. A fast optical pulse incident on the emitter produces a group of carriers, which then diffuses toward the junction. During this process, recombination may occur at the front surface as well as in the bulk. A current pulse is produced at the device terminals when the modified carrier group reaches the junction. The time delay between excitation and current output reflects the minority carrier mobility, while the slope of the current pulse contains information about S and τ. This information is particularly useful for analysis of radiation damaged devices since it probes material properties directly rather than
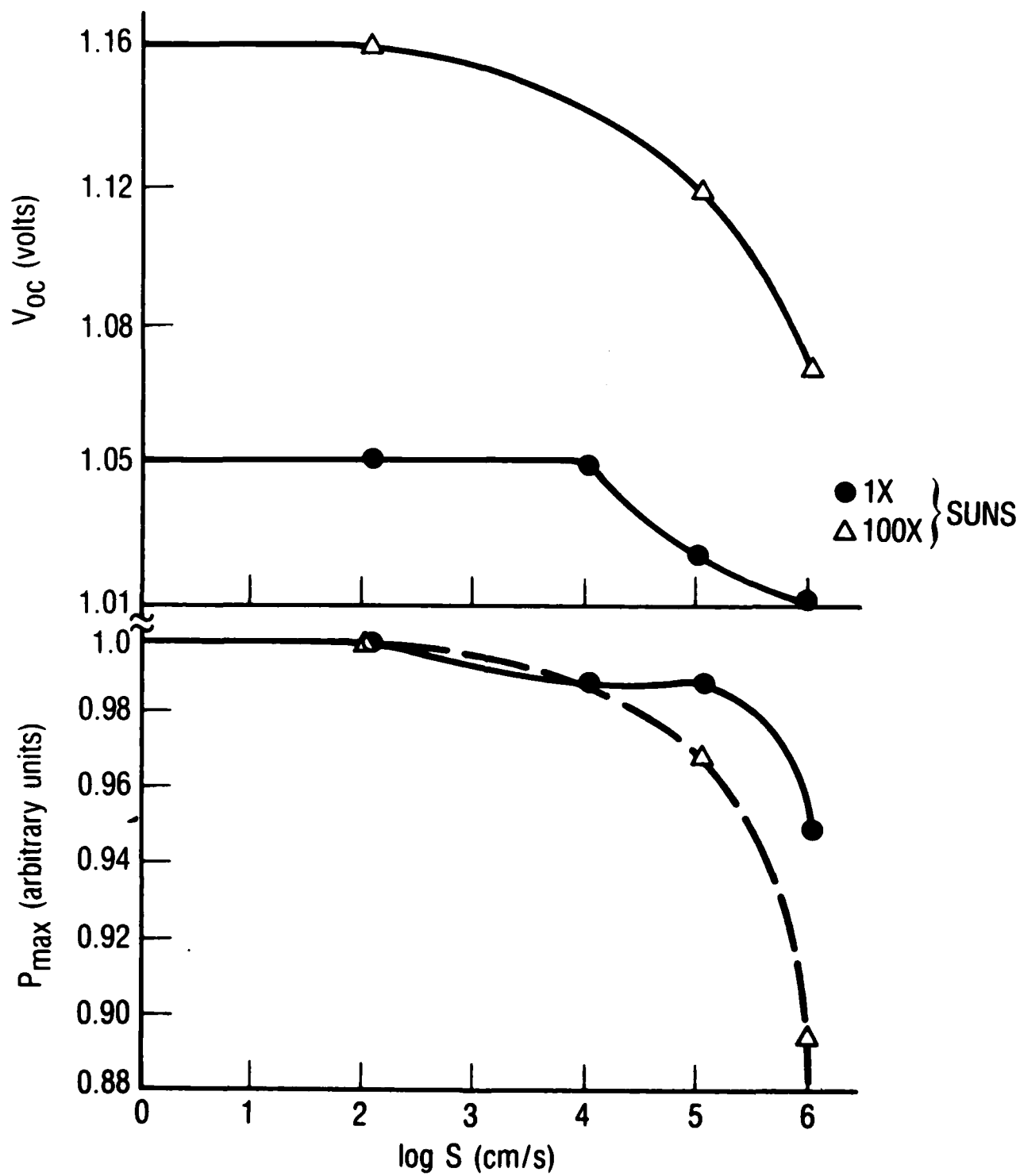
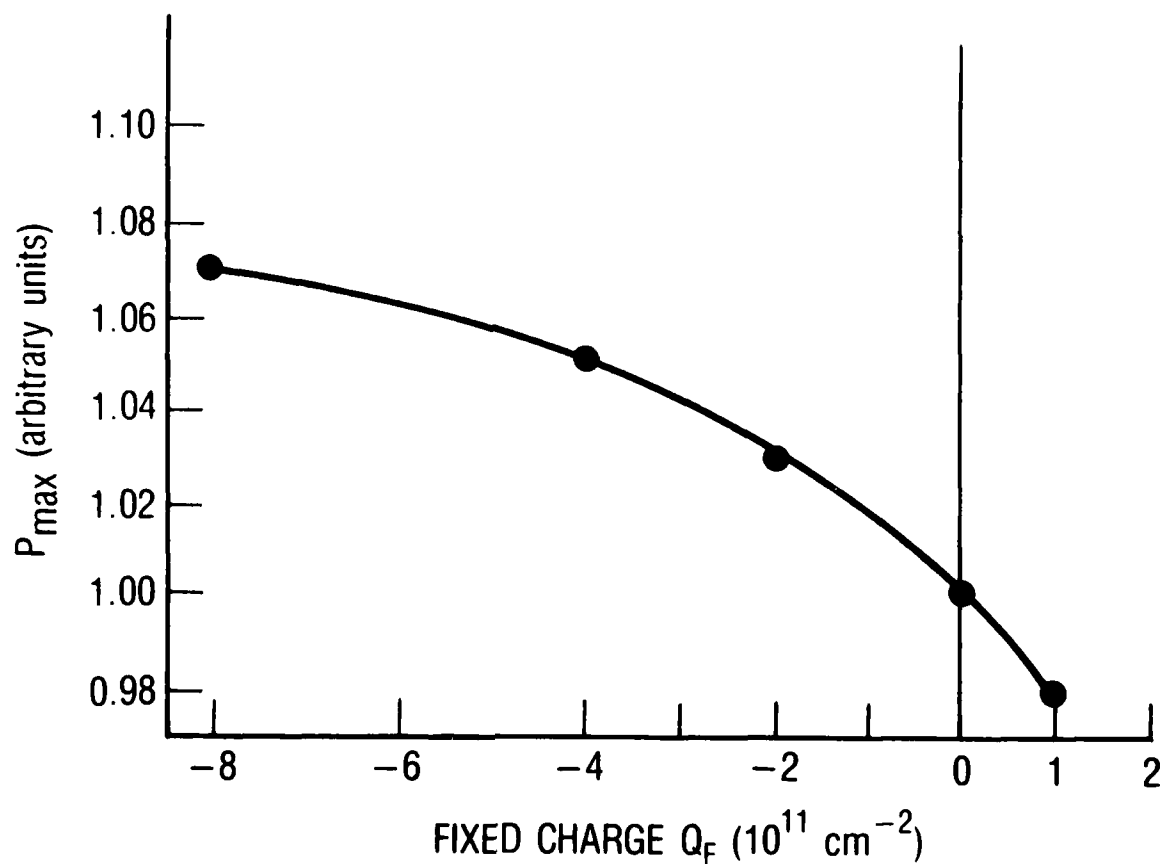Fig. 8. Power and Voltage for Cell with Selective Ohmic Contact

Fig. 9. Effect of Fixed Surface Charge on Output Power

device properties. PISCES can simulate this experiment. Figure 10 shows the current pulse resulting from a PISCES transient simulation on an n/p solar cell with a 1.56 μm thick emitter. The optical excitation at t = 0 was a delta function pulse, with wavelength approximately 510 nm so that the initial carrier group was very localized near the emitter surface. The output pulse is seen to have significant width, from which the material parameters S and τ may by estimated. The minority carrier diffusivity is obtained from the time delay value of 0.2 ns.
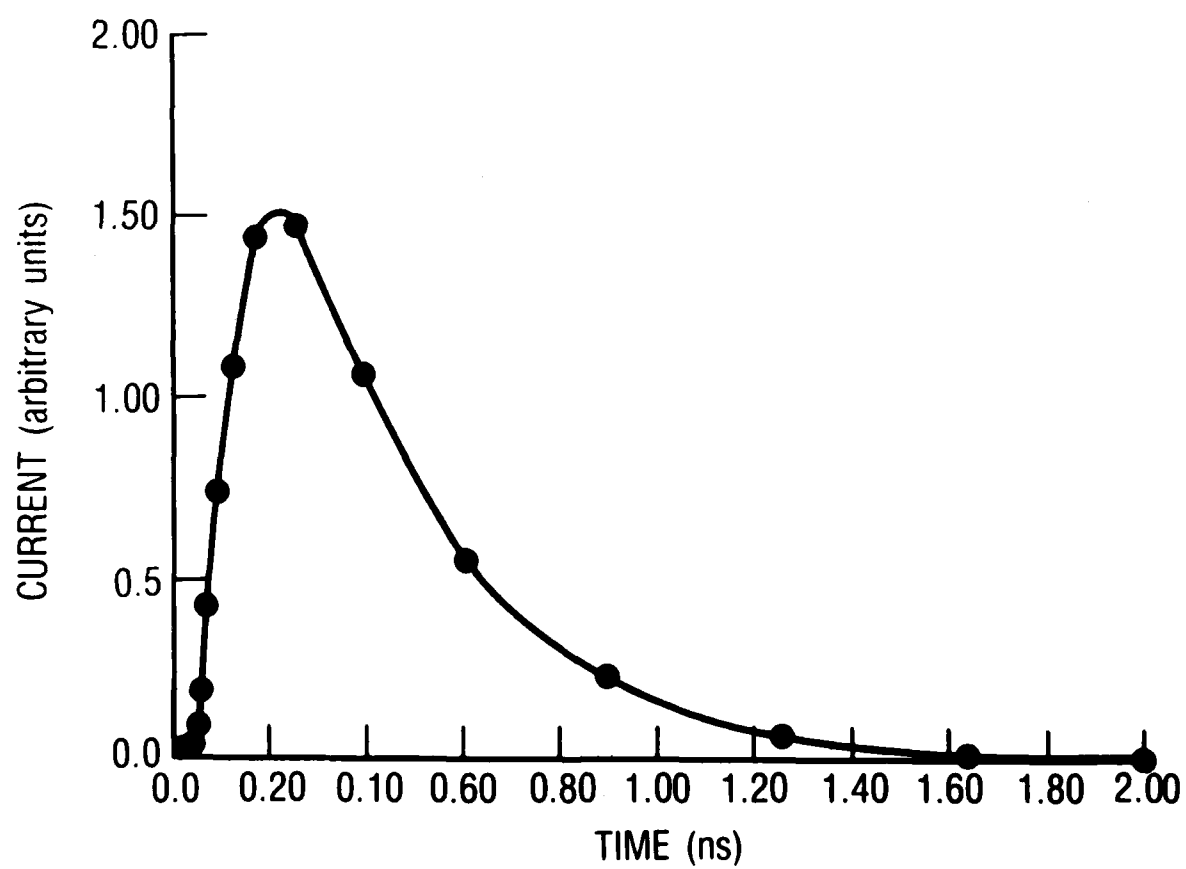
Fig. 10.   Time of Flight Current Profile

5. SUMMARY

The PISCES computer code is an extremely useful method of analyzing the performance of semiconductor devices. The modifications which allow optical generation processes to be included open the entire range of solar cell structures for investigation. A number of examples have been described which treated variables such as minority carrier bulk and surface recombination, excitation wavelength, and transient response. The relationship of these parameters to cell performance have been described and their use in the cell optimization process demonstrated. Particular applications of this capability include (a) the analysis of novel cell designs, such as point contact GaAs cells, and (b) sensitivity analyis of cell degradation processes. Of special interest is the degradation of cell output as the result of radiation exposure, which reduces the carrier lifetimes and also has significant effects on surface recombination.

6. REFERENCES

1. S. J. Fonash, <u>Solar Cell Device Physics</u>, Academic Press (1981), pg. 129.

2. J.G. Rollins, <u>Modification and Use of the PISCES-II Device Simulation Program for Analyzing Single Event Effects</u>, ATR-85(8040-02)-1.

3. D.C. Marvin, et al, <u>Picosecond Carrier Dynamics Near the Gallium Arsenide Surface</u>, TR0086A(2945-01)-5.

LABORATORY OPERATIONS

The Aerospace Corporation functions as an "architect-engineer" for national security projects, specializing in advanced military space systems. Providing research support, the corporation's Laboratory Operations conducts experimental and theoretical investigations that focus on the application of scientific and technical advances to such systems. Vital to the success of these investigations is the technical staff's wide-ranging expertise and its ability to stay current with new developments. This expertise is enhanced by a research program aimed at dealing with the many problems associated with rapidly evolving space systems. Contributing their capabilities to the research effort are these individual laboratories:

Aerophysics Laboratory: Launch vehicle and reentry fluid mechanics, heat transfer and flight dynamics; chemical and electric propulsion, propellant chemistry, chemical dynamics, environmental chemistry, trace detection; spacecraft structural mechanics, contamination, thermal and structural control; high temperature thermomechanics, gas kinetics and radiation; cw and pulsed chemical and excimer laser development including chemical kinetics, spectroscopy, optical resonators, beam control, atmospheric propagation, laser effects and countermeasures.

Chemistry and Physics Laboratory: Atmospheric chemical reactions, atmospheric optics, light scattering, state-specific chemical reactions and radiative signatures of missile plumes, sensor out-of-field-of-view rejection, applied laser spectroscopy, laser chemistry, laser optoelectronics, solar cell physics, battery electrochemistry, space vacuum and radiation effects on materials, lubrication and surface phenomena, thermionic emission, photo-sensitive materials and detectors, atomic frequency standards, and environmental chemistry.

Computer Science Laboratory: Program verification, program translation, performance-sensitive system design, distributed architectures for spaceborne computers, fault-tolerant computer systems, artificial intelligence, micro-electronics applications, communication protocols, and computer security.

Electronics Research Laboratory: Microelectronics, solid-state device physics, compound semiconductors, radiation hardening; electro-optics, quantum electronics, solid-state lasers, optical propagation and communications; microwave semiconductor devices, microwave/millimeter wave measurements, diagnostics and radiometry, microwave/millimeter wave thermionic devices; atomic time and frequency standards; antennas, rf systems, electromagnetic propagation phenomena, space communication systems.

Materials Sciences Laboratory: Development of new materials: metals, alloys, ceramics, polymers and their composites, and new forms of carbon; non-destructive evaluation, component failure analysis and reliability; fracture mechanics and stress corrosion; analysis and evaluation of materials at cryogenic and elevated temperatures as well as in space and enemy-induced environments.

Space Sciences Laboratory: Magnetospheric, auroral and cosmic ray physics, wave-particle interactions, magnetospheric plasma waves; atmospheric and ionospheric physics, density and composition of the upper atmosphere, remote sensing using atmospheric radiation; solar physics, infrared astronomy, infrared signature analysis; effects of solar activity, magnetic storms and nuclear explosions on the earth's atmosphere, ionosphere and magnetosphere; effects of electromagnetic and particulate radiations on space systems; space instrumentation.

...